Computational Modeling of a Mechanized Benchtop Apparatus for Leading-Edge Slat Noise Treatment Device Prototypes

Travis L. Turner[1] and James B. Moore[2]
NASA Langley Research Center, Hampton, VA, 23681

David L. Long[3]
Analytical Mechanics Associates, Hampton, VA 23666

Airframe noise is a growing concern in the vicinity of airports because of population growth and gains in engine noise reduction that have rendered the airframe an equal contributor during the approach and landing phases of flight for many transport aircraft. The leading-edge-slat device of a typical high-lift system for transport aircraft is a prominent source of airframe noise. Two technologies have significant potential for slat noise reduction; the slat-cove filler (SCF) and the slat-gap filler (SGF). Previous work was done on a 2D section of a transport-aircraft wing to demonstrate the implementation feasibility of these concepts. Benchtop hardware was developed in that work for qualitative parametric study. The benchtop models were mechanized for quantitative measurements of performance. Computational models of the mechanized benchtop apparatus for the SCF were developed and the performance of the system for five different SCF assemblies is demonstrated.

Nomenclature

E_A,E_M	=	Austenite/Martensite Young's modulus
$\nu A, \nu M$	=	Austenite/Martensite Poisson's ratio
σ^{Ms}, σ^{Mf}	=	critical stress to start/finish the Martensite transformation
σ_c^{Ms}	=	critical stress to start/finish the Martensite transformation
σ^{As}, σ^{Af}	=	critical stress to start/finish the Austenite transformation
C_A,C_M	=	Austenite/Martensite Young's modulus
H	=	transformation strain
T_o	=	reference temperature
SMA	=	shape memory alloy
SCF	=	slat-cove filler
SGF	=	slat-gap filler
AoA	=	angle of attack
C_L	=	lift coefficient
DLE	=	drooped leading edge
OML	=	outer moldline

I. Introduction

AIRFRAME noise is the component of aircraft noise not attributable to the engines. Airframe noise is particularly important for environmental and community impact in the approach and landing phases of flight because of progress in reducing engine noise and the fact that the engines are typically operating at reduced power under those flight conditions. The high-lift system of typical transport aircraft is a major contributor to airframe noise and the leading-edge slat is a prominent noise-producing, high-lift device.

[1] Research Engineer, Structural Acoustics Branch, 2 N Dryden Street/Mail Stop 463, AIAA Senior Member
[2] Research Engineer, Structural Mechanics and Concepts Branch/Mail Stop 190
[3] Designer III, TEAMS2 – Structural Dynamics Branch, 4B W Taylor Street/Mail Stop 230

Many transport-class aircraft incorporate leading-edge-slat and trailing-edge-flap, high-lift devices that are separated from the main wing in the high-lift configuration, as indicated by the slat and main wing in Figure 1, because this configuration can achieve much greater lift than a contiguous (gapless), high-lift configuration represented by the connecting structure (dashed line) shown in Figure 2. However, the separated slat presents many geometric discontinuities to the flow, which is the cause for considerable unsteadiness and noise production in the flow.

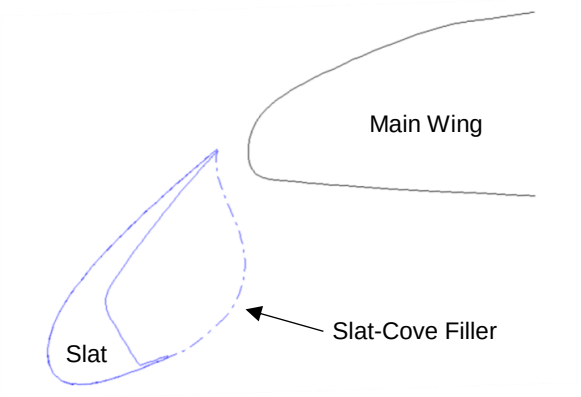

Figure 1. Schematic of a slat device separated from the main wing, typical of modern transport aircraft, with a notional slat-cove filler.

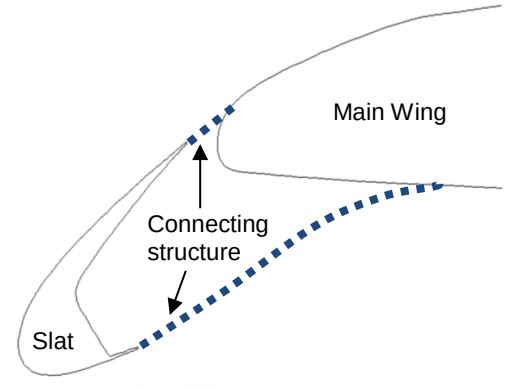

Figure 2. Notional schematic of a gapless high-lift system or a drooped leading edge.

A graphic of the flow characteristics in the vicinity of a deployed, leading-edge slat is shown in Figure 3[1]. The flow splits at the stagnation point on the slat and the flow progressing on the lower surface separates from the slat at the cusp and forms a shear layer that reattaches at the top of the slat cove, thereby bounding a vortical recirculation region in the cove. These flow features, and their interaction with the structure, support many unsteady phenomena that are sources for radiated acoustic noise[1-6]. Significant research effort has been expended in developing concepts and approaches for reduction of leading-edge-slat noise without compromising cruise efficiency or the lift and stall characteristics at landing.

II. Slat Noise Reduction Concepts

Several concepts have been proposed for reducing slat noise while maintaining the gap to avoid compromise of the aerodynamic performance. These include brushes[2], serrated cusps and extended blade seals[7], and slat-cove fillers (SCFs)[8,9]. Brushes result in added drag at cruise and the noise benefit is marginal. Neither the serrated slat cusp nor the extended blade seal resulted in significant noise reduction in a wind tunnel test[10]. The SCF concept has been shown, both experimentally[9,10] and computationally[11], to significantly reduce slat noise.

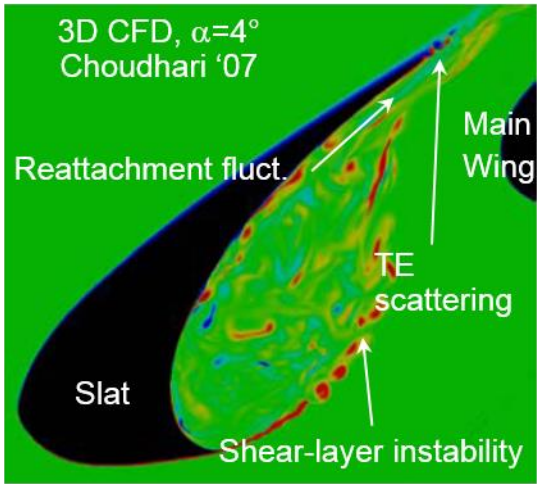

Figure 3. Flow vorticity in the vicinity of a deployed, leading-edge-slat device[1].

A notional SCF of optimal shape to minimize noise is shown in Figure 1. The SCF guides the flow through the slat-wing gap such that unsteadiness in the flow is reduced. Previous work was done, based upon the optimal SCF profile in Figure 1, to develop a flexible, SCF structure that passively and autonomously achieves the highly-disparate deployed and retracted configurations simply by movement of the slat actuator[12]. A concept consisting of one or more superelastic shape memory alloy (SMA) components, shape set to the deployed configuration, was found to satisfy the application requirements and provide implementation feasibility. Further work was done to optimize the superelastic-SMA, SCF design to minimize the actuation authority required to stow the structure while satisfying steady-aerodynamic-load and other requirements[13,14]. Recent work has studied

means to further reduce actuation requirements[15]. Study of the static and dynamic, fluid-structure-interaction (FSI) behavior of the highly-flexible SCF structural system has also recently been undertaken[16].

The noise benefit of treatments that maintain the separated (gapped) slat is limited by the fact that the flow between the deployed slat and the main wing is maintained, along with some of the noise production mechanisms. It is desirable, from an aeroacoustic noise perspective, to eliminate the flow between the slat and main wing to minimize the noise production mechanisms and maximize the noise benefit. A class of structural concepts of this type, known as drooped leading edge (DLE) concepts, are represented by the schematic in Figure 2 and have been proposed and studied by various research groups specifically to investigate the possibility of eliminating the slat-gap flow[17-22].

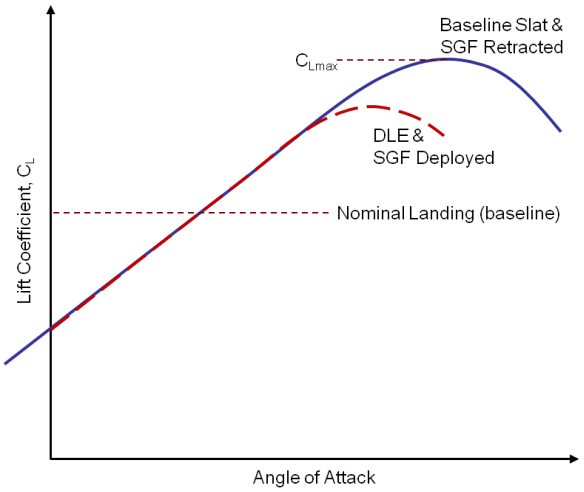

Figure 4. Representative plot of lift coefficient versus angle of attack.

Typical DLE systems represent a significant weight addition because of the extensive added structure and accompanying actuation requirements. More importantly, DLE systems cannot achieve the required lift and stall performance at high angle of attack (AoA) because they negate the advantage of a multielement, high-lift system. This effect is illustrated in the representative plot of lift coefficient versus angle of attack (AoA) in Figure 4. Known attempts to overcome this deficit, such as via active flow control, have suffered from excessive weight, infeasible implementation and/or other negative effects.

Recognition that the lift performance of DLE systems is equivalent to the baseline for all typical angles of attack and the deficit only occurs at high angles, corresponding to atypical or emergency conditions, suggests that a gap-on-demand system is ideal for this application. The slat-gap-filler (SGF) concept, shown schematically in Figure 5, was proposed to achieve a gap-on-demand system. It was envisioned that the SGF would block the gap flow under all normal operating conditions, thereby minimizing noise without aerodynamic compromise, but could be opened in atypical/emergency conditions to achieve optimized lift performance at the expense of increased noise at a time when noise is not a primary concern.

Recent experiments demonstrated that closing the slat gap practically eliminates the noise from the slat component[23]. The small structural addition required by the SGF concept was seen as simultaneously mechanically feasible for implementation, defeatable in emergency and with minimal weight addition. Previous work was done to study possible SGF implementation approaches including mechanized and deformable concepts[24]. The approach that best met the design requirements and constraints involved utilizing a portion of the skin on the leading edge of the main wing as a deformable, reconfigurable structure with the potentially large deformation enabled by superelastic SMA materials. The SGF could be secured to the main wing at one end, actuated by a mechanism at the other and could be minimum gauge since it only needs to sustain local aerodynamic loads. Thus, the SGF was envisioned to overlay the stressed skin, as shown in Figure 6.

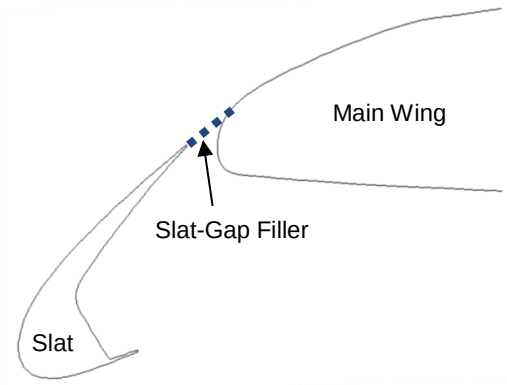

Figure 5. Notional simplified gapless, high-lift system; the slat-gap filler.

III. Benchtop Models

Benchtop models were developed as part of the SCF[12] and SGF[24] studies to explore practical implementation challenges, to quantify actuator authority requirements on a simplified system, and to allow parametric study with physical hardware. The requirement for both concepts to deploy and retract with the slat made it practical and desirable

for authority from the slat actuator to be used. A schematic of a slat actuator typical of modern transport aircraft is shown in Figure 7, where the slat is shown actuated by a pinion driving a gear rack integrated with the slat track. The design of the benchtop models was based upon the transport-wing geometry shown in Figure 1 and the actuation system was motivated by that shown in Figure 7. The resulting benchtop models are shown in the CAD graphics for the SCF in Figure 8 and for the SGF in Figures 9 and 10. The models represent a thin (0.75 inch) spanwise-uniform section from the airfoil in Figure 1 to facilitate rapid parametric study and to accommodate limitations in the component sizes for superelastic SMA components that were available from suppliers.

Hardware common to both the SCF and the SGF system included the baseplate, main wing, slat, slat track with gear rack, pinion gear and drive assembly. The main wing was fixed to the baseplate. Two stud bearings were mounted on the back side of the slat and inserted into slots in the baseplate that enforced movement of the slat along a circular arc relative to the main wing. Ball transfers, pressed into the slat, reduced the friction between the opposing slat and baseplate surfaces. The slat track was fastened to the slat and mated with the pinion in a manner representative of typical flight hardware, e.g., Figure 7. The position of the slat track was enforced at the pinion engagement location, thereby maintaining gear engagement, by a stud bearing protruding from the baseplate and into a slot in the slat track. Note that the slat track did not have to take significant bending loads, that would typically be accommodated by the roller arrangement in flight hardware (Figure 7), because of the slat bearings in the benchtop model. A sleeve bushing and a thrust bearing reduced the friction in the rotation of the pinion. The pinion was driven by an assembly consisting of a stepper motor, gear reducer and a torque transducer, shown on the SGF benchtop assembly in Figure 10.

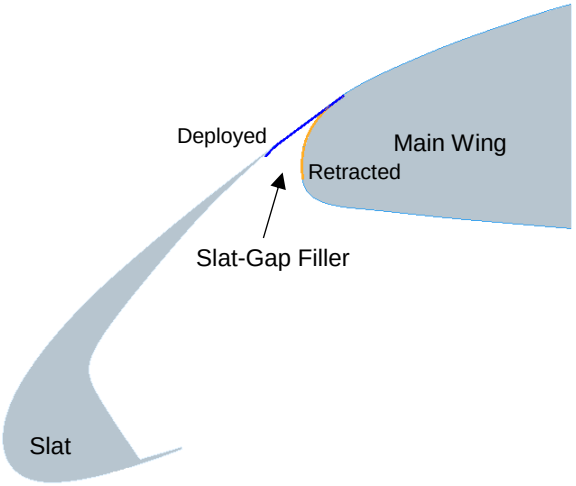

Figure 6. Schematic of the SGF concept involving a deployable-skin overlay on the main wing.

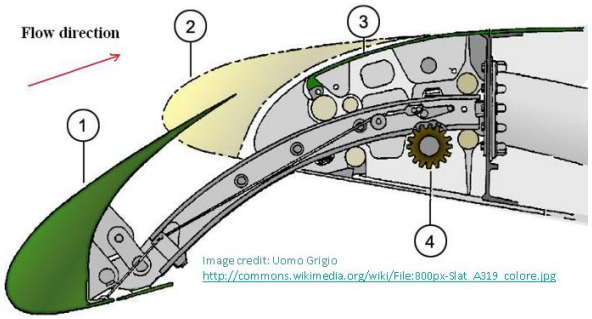

Figure 7. Graphic of an electromechanically-actuated, leading-edge slat.

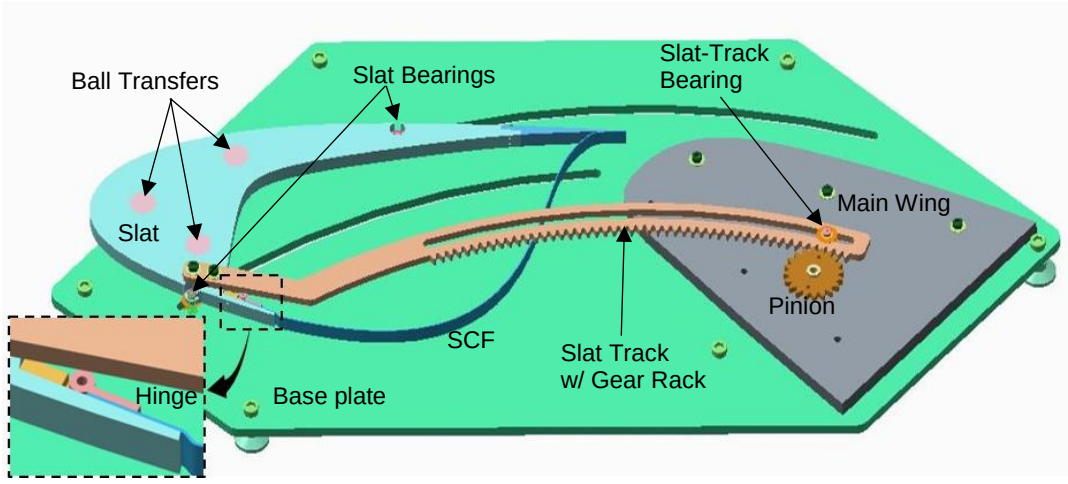

Figure 8. CAD model for the mechanized SCF benchtop model. Inset shows close-up of hinge.

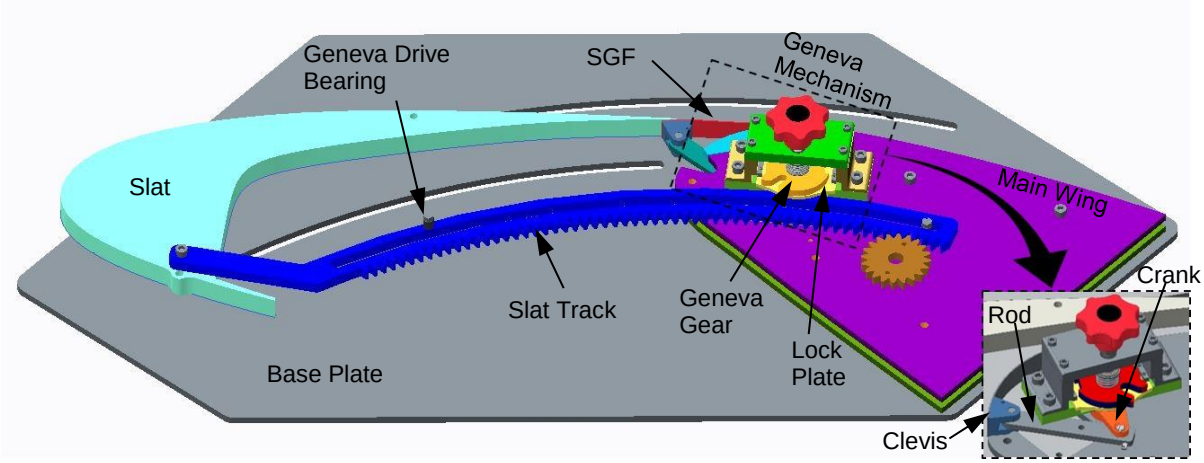

Figure 9. CAD model for the mechanized SGF benchtop model; SGF deployed. Inset shows retracted SGF & Geneva assembly without top-main-wing plate, revealing 3-bar mechanism: crank, rod and clevis.

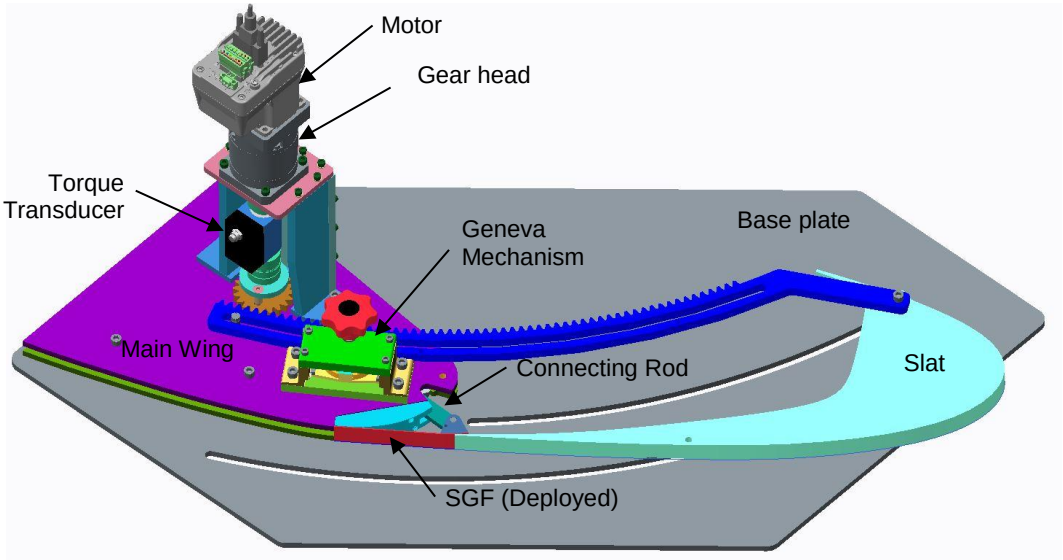

Figure 10. Top view of the CAD model for the mechanized SGF benchtop model with the drive mechanism.

The slat-cove filler, shown in Figure 8, was attached to the slat near the cusp, or lower trailing edge, by a hinge and at the upper trailing edge by a riveted lap joint. As mentioned in Section II, simplified physical and computational models were used for parametric study and optimization of the SCF for this 2D airframe, where optimization entailed minimizing the actuator authority required to stow the SCF while satisfying static load and other constraints[12-14]. Multipiece SCF assemblies, consisting of two SMA flexures separated by a stiffer mid-link, were considered in those studies because of the possibility for controlling the deformation distribution and, consequently, the stowage timing. Although the optimal SCF configuration for this 2D airframe case proved to be a monolithic (one-piece), superelastic SMA with the shortest hinge possible, other SCF configurations that satisfied the application requirements were found in the course of the parametric study and optimization[13,14]. Four of these suboptimal but operable configurations (Mono-2 through Multi-3) are shown with the optimal design (Mono-1) in Figure 11, where the reference lines and dimensions are consistent with the parametric computational model used for the optimization. The closest, suboptimal design also consisted of a monolithic flexure, but with a longer hinge that reduced the flexible length of the SCF and, consequently, the mobility during stowage. The other three designs were multipiece SCF assemblies with varying mid-link length, mid-link position and hinge length that resulted in differing strain-energy distributions and stowage timing. Although it was not advantageous for the present airframe geometry, the presence of the mid-link could be advantageous for other airframe geometries. The five SCF assemblies shown in Figure 11 were selected because they span significant ranges of required actuator authority and SCF stowage timing. All five SCF assemblies were

fabricated for testing on the benchtop and modeled in this work to study their relative responses. It was felt that the ranges in response would offer a broad basis for validation of the computational models with experimental measurements.

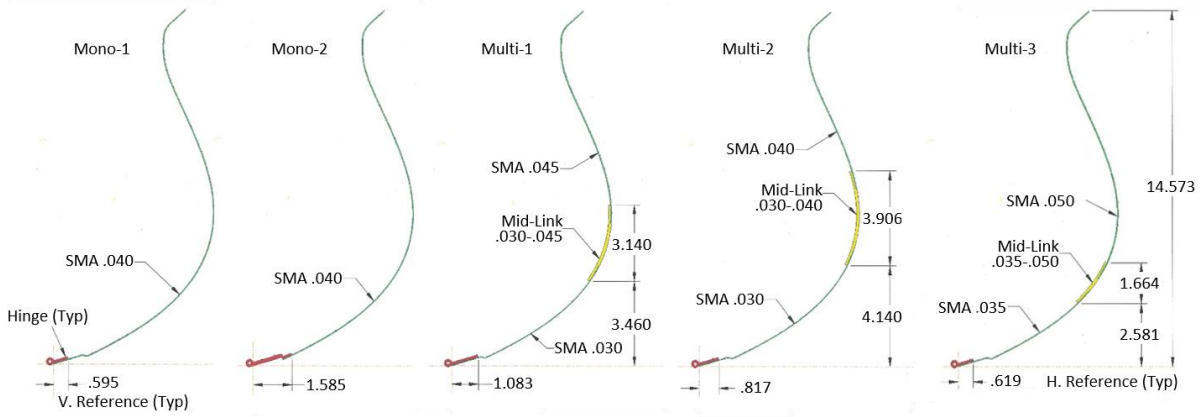

Figure 11. Schematic of optimal (Mono-1) SCF assembly with four suboptimal assemblies including essential component and dimension information for each.

The SGF benchtop apparatus included additional components, and corresponding complexity, for actuation of the SGF, as shown in Figure 9. The SGF actuation mechanism consisted of a stud bearing on the slat track that engaged a Geneva gear as the slat track moved during slat actuation. Engagement of the Geneva gear rotated a crank shaft that drove a connecting rod. The connecting rod terminated at a clevis that was attached to the moving end of the SGF, thereby completing a 3-bar mechanism. The bearing on the slat track also contacted a locking plate with a tang that engaged one of two detents to secure the Geneva gear either in the deployed or retracted position. The Geneva mechanism included an emergency button to simulate mechanized disengagement of the SGF from the slat actuator, thereby allowing the slat gap to be opened independent of slat position and movement. The mechanism was designed to reset at the next full slat retraction. The main wing in the SGF assembly consisted of two plates separated by a gap where the crank, connecting rod, and associated connections were housed, as shown in the inset of Figure 9.

Note that actuation of the slat brings the SCF into/out of contact with the main wing for stowage/deployment so that slat actuator authority is used directly to manipulate the SCF in conjunction with the slat. The SGF actuation mechanism was designed to direct actuation authority from the slat actuator to the SGF via the Geneva assembly, thereby ganging SGF actuation to the slat in a manner that can be disengaged when required.

IV. Computational Models

Simplified computational models were previously developed to analyze the SCF[12-16] and SGF[24] performance under aerodynamic and retract/deploy loads. The objectives of the present work were to develop finite element (FE) models of the mechanized benchtop SCF and SGF apparatus for refined prediction of the structural performance, practical estimation of actuator authority requirements, and eventual comparison with experimental results. Models presented in this document will be limited to the SCF cases. The FE models were developed in Abaqus because of the built-in constitutive model for superelastic SMAs and the comprehensive and robust capability for analysis of complex contact and large deformation mechanics.

The representative FE model shown in Figure 12 was built using the CAD geometry in Figure 8. The model was simplified by considering the baseplate, main wing, slat, hinge and bearings to be rigid and only the SCF components were deformable. The size of the FE model was reduced by meshing only essential components. Consequently, the outer mold line (OML) of the main wing and the bounding surfaces of the baseplate slots were the only surfaces meshed for those components. Additional instances of the main wing and baseplate were included as *Display Bodies*[4] for visualization.

The rigid components were modeled as shells and assigned rigid-body constraints, each with a *Reference Point* that governed its movement. The baseplate slots and main-wing OML were constrained to be motionless. The pinion was assigned an enforced rotation of 13.36 radians (2.126 revolutions) about the z-axis so as to drive the entire system from the fully-deployed to the fully-retracted configuration. The slat track was assigned z-symmetry

[4] Italicized text designates modeling features or key words in Abaqus.

(U3=UR1=UR2=0) constraints to force the slat track to move in a plane parallel to the main wing and baseplate. The slat-track imposed similar constraints on the slat and SCF component(s) implicitly due to a *Tie Constraint* between the slat track and the slat and the following additional constraints. The hinge mount was removed from the model and replaced by an idealized analog consisting of a *Beam Connector* to bind the hinge axis to the slat motion and a *Hinge Connector* to allow the rigid-body-hinge component to rotate about its axis. The SCF was assigned *Tie Constraints* to the hinge and to the cove surface of the slat near the trailing edge. The slat-track bearing was affixed appropriately to the main wing component, but allowed to rotate about the z-axis. The *Reference Points* for the slat bearings were assigned *Tie Constraints* to the bottom surface of the slat. This constraint prevented them from simulating rolling contact, but the *Interaction Properties* with the baseplate slots were adjusted to account for that, as described subsequently.

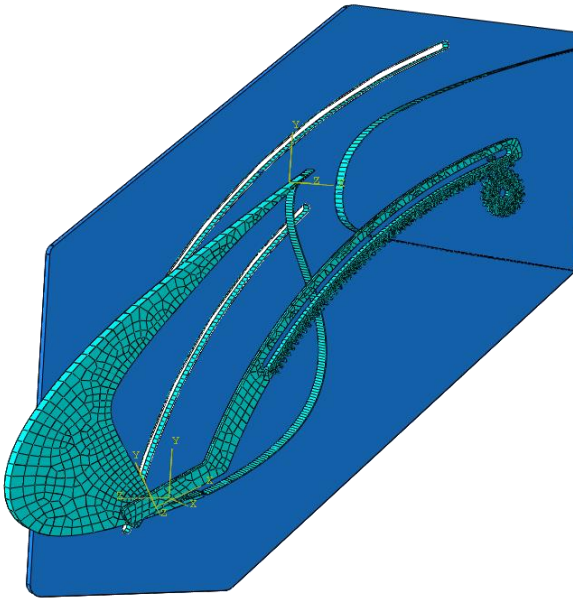

Figure 12. FEM of the SCF benchtop apparatus with the TE2Hinge SCF installed.

Contact Pairs were established between the pinion and gear rack, the slat track and its slot bearing, the slat bearings and the baseplate slots, the SCF and the slat cove and the SCF and the main-wing OML. In each case, the normal behavior was modeled by a *Linear, Pressure-Overclosure* constraint. The tangential behavior of the gear engagement and the rolling contact of the bearing in the slat-track slot was modeled by a *Penalty Friction* formulation with an *Isotropic* friction coefficient of 5%. The tangential behavior of the slat-bearings in the baseplate slots was modeled as frictionless because the rolling behavior of the bearings was suppressed by the *Tie Constraint* to the slat. The *Contact Interaction* of the SCF with the slat cove and main wing was also modeled as frictionless because of the Teflon treatment to those surfaces on the benchtop model and anticipated, similar treatment for flight hardware.

The rigid components were modeled with S4R and S3 elements with spatial resolution dictated by geometric representation and contact considerations. The spatial resolution on the slat cove and main-wing-OML surfaces was 0.2 inches in the chordwise direction to assure reasonable accuracy in contact simulation with the curved surfaces. The spatial resolution on the bounding surfaces of the baseplate slots and the slot in the slat track was also 0.2 inches for *Contact Interaction* with the rigid-body bearings. All of the aforementioned rigid components needed only a single element in the spanwise direction because of the spanwise-uniform geometry. The spatial resolution on the hinge and bearing components was nominally 0.04 inches, which was driven by the dimensions of the components. Similarly, the spatial resolution on the gear rack and pinion were nominally 0.04 inches near the contact surfaces of the teeth, to accurately represent the geometry and contact mechanics, while it was coarser elsewhere.

Table 1. Material properties for analysis of the superelastic SMA via the built-in model in Abaqus, based upon the Auricchio model[25,26]. Values were determined in previous work[13,14].

Property	Value
E_A	7086 ksi
E_M	5798 ksi
ν_A, ν_M	0.33
ρ	6.03e-4 lbf·s^2/in^4
$\sigma^{Ms}, \sigma_c^{Ms}$	68.3 ksi
σ^{Mf}	74.6 ksi
σ^{As}	28.5 ksi
σ^{Af}	24.0 ksi
C^A, C^M	805.6 psi/°F
H	4.45%
To	75 °F

The flexures were modeled with S4R shell elements and assigned superelastic SMA material properties through the *User Material* constitutive model built-in to Abaqus, which is an implementation of the model developed by Auricchio and coauthors[25,26]. Material properties required to quantify the constitutive model for the NiTi material used in the benchtop apparatus were acquired in previous, related work and are shown in Table 1[13,14]. The flexure mesh provided a spatial resolution of 0.125 inches in the chordwise direction, which was conservative but enabled options for higher-fidelity modeling, e.g., incorporating fasteners, for the joints between the SCF and the hinge and/or slat cove at the trailing edge. A single element dimension in the spanwise direction was found to be adequate for the flexures and this approach was combined with z-symmetry

boundary conditions on both spanwise edges of the SCF flexure. The flexure spatial resolution also was determined to be compatible with that of the main-wing-OML and slat-cove for contact simulation. When relevant to the analysis, the mid-link was modeled as an elastic solid with C3D8R elements and material properties (E=30 Msi, ν=0.26 and ρ=7.4e-4 lbf·s^2/in^4) corresponding to the stainless steel used for these components in the physical models. Note that stainless steel would not typically be used in a flight application, but it was convenient for the benchtop hardware.

Analysis of each SCF assembly on the benchtop apparatus was conducted with a *Dynamic, Implicit Step* with a step time of 10 seconds and an imposed pinion rotational displacement of 13.36 radians. This time period was considered to be at the faster end of an acceptable range for slat articulation on a typical transport aircraft. The *Quasi-Static Application* type was selected to stabilize the system during dynamic, e.g., snap-through, events that may occur during SCF stowage and avoid potentially excessive computational expense involved in attempting to resolve such highly-dynamic behavior.

V. Results

The input torque at the pinion, corresponding to the z-axis reaction moment at the pinion reference point, required to drive the apparatus from the fully-deployed configuration to the fully-retracted configuration is shown in Figure 13 for each of the SCF assemblies. Ignoring the spurious spikes in the data, it can be seen that the Mono-1 assembly requires the lowest peak input torque. The Mono-2 assembly requires slightly more torque in the early contact with the main wing, at around 3 seconds in the analysis, and requires significantly more torque just prior to the SCF snapping into the slat cove at about 8.1 seconds. It can also be seen that the Multi-1 and Multi-2 multipiece SCF assemblies snap into the slat cove earlier in the retraction sequence, at about 5.4 and 6.1 seconds, respectively, than the monolithic designs. This difference in timing is due to contact between the stiff mid-link and the main wing forcing the lower part of the SCF into the cove more quickly. Consequently, the Multi-1 and Multi-2 assemblies require a similar or lower integrated torque, but the peak torque requirement is almost double that of the monolithic designs. The short and forward-placed mid-link in the Multi-3 SCF assembly does not result in earlier stowage and, thus, the assembly requires the highest peak torque as well as the highest integrated torque.

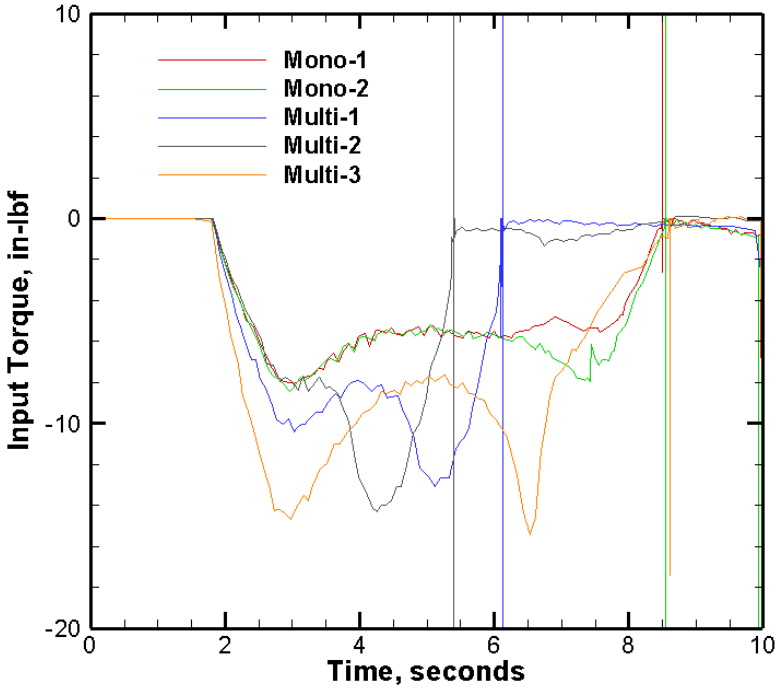

Figure 13. Input torque at the pinion versus time for the five SCF assemblies.

The spikes in input torque that appear late in the stowage sequence of each assembly are associated with inertial effects during a dynamic event when the SCF snaps into the slat cove. This effect can be seen in the representative plot of internal and kinetic energy in the Mono-1 assembly shown in Figure 14. A drop in internal energy in the system, indicative of stress/strain relaxation in the deformable component (the SMA flexure), occurs simultaneously with a brief spike in kinetic energy. The magnitude of the kinetic energy spike is not quantitatively correct due to the *Quasi-Static Application* type of the analysis stabilizing the solution artificially and leaving the calculation of such events unresolved computationally.

VI. Conclusions

Airframe noise has become a significant problem for the future of transport aircraft operations because of the increasing populations in the vicinity of airports and because progress in engine noise reduction has rendered airframe

noise an equal contributor during the approach and landing phases of flight for many aircraft. The noise problem associated with the leading-edge-slat, high-lift device was described and the technologies proposed for reducing the slat noise were reviewed. The promise of two slat-noise treatments, the slat-cove filler (SCF) and slat-gap filler (SGF), was substantiated. The SCF fills the slat cove with a flexible, reconfigurable structure that guides the flow in a manner that reduces the unsteadiness and the radiated noise while remaining flexible enough to reconfigure and stow between the slat and main wing for cruise. The SGF blocks the gap flow via a reconfigurable overleaf of skin structure on the leading edge of the main wing. The resulting configuration achieves lift characteristics at angles of attack suitable for landing, but can be disengaged from the slat movement, to open the gap, at anomalous angles to regain the baseline lift and stall characteristics. The SGF promises greater noise reduction at the expense of greater mechanical complexity. Superelastic shape memory alloys (SMAs) were proposed to enable the large deformation required for both concepts.

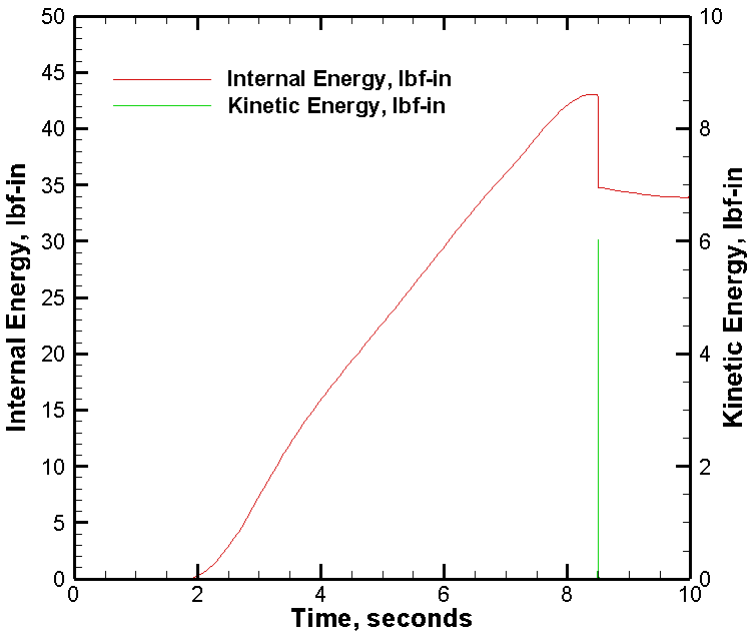

Figure 14. Internal and kinetic energy in the finite element model of the benchtop apparatus with the Mono-1 SCF assembly.

Previous studies demonstrated the feasibility of the SCF and SGF concepts on a thin spanwise-uniform slice of a transport-class airframe, and described optimal SCF and SGF designs for the 2D airframe studied. Benchtop models for the SCF and SGF concepts were developed as part of those studies and recent activity has been aimed at mechanizing these benchtop models to quantify the performance of the prototypes. The objective of the present work was to develop computational models of the benchtop hardware for comparison with experimental measurements of the actuator requirements and enable extension of the prototype designs to 3D configurations.

The benchtop model designs for the SCF and SGF systems were discussed in detail. They include representation of the forward 10% of the main wing, the slat, the slat track, the drive mechanism, the SCF and SGF structures and an auxiliary mechanism for SGF articulation with the slat. Computational models of the benchtop hardware were developed in Abaqus to predict the system performance. The modeling approach included simplifications of rigid-body constraints for the main wing, slat and slat actuation system, but high-fidelity representations of the SCF assembly. The Abaqus-native model for superelastic SMA materials was employed. Simulations results were limited to the SCF apparatus and included the performance for five different SCF assemblies. The five assemblies were identified in previous work using simplified computational models for parametric study and optimization and included the optimal design and four suboptimal designs that met the application requirements and constraints. Implicit dynamic simulations were conducted with the *Quasi-Static* application in Abaqus to stabilize the solution to dynamic phenomena such as snap-through of the superelastic component.

The simulation indicated that the optimal design of a monolithic SMA SCF required a peak torque of approximately eight in-lbf from the drive motor for the slat actuator. Two of the multipiece SCF assemblies required less integrated torque relative to the optimal design, although the peak torque requirement was approximately double. This behavior was due to the stiff mid-link forcing the forward part of the SCF to retract early. All of the SCF assemblies exhibited a snapping behavior at the completion of SCF stowage. This behavior was manifested as a spurious spike in drive torque because the *Quasi-Static* application in the simulation stabilized the solution without resolving the dynamic behavior. The presence of the dynamic behavior was confirmed by examination of the internal and kinetic energies during the simulations.

Improvements in model fidelity will likely be required for successful correlation with experimental measurements. Improvements could include modeling the inertial effects of the slat, slat track, hinge and pinion. Refinements to the contact interactions could include friction coefficients determined by experiment. Elasticity of the slat may also be a factor. Simulations of the SGF apparatus will be completed using a modeling approach similar to that described here.

These computational models will be correlated with experimental measurements from the benchtop apparatus. The resulting validated computational models will then be used to predict the actuator authority requirements for practical 3D wing structures and commensurate SCF and SGF treatments.

Acknowledgments

David Lockard, Medhi Khorrami, Craig Streett and Meelan Choudhari (NASA LaRC) provided valuable guidance on requirements of the application and on aerodynamics/aeroacoustics in general and they were valuable collaborators on concept development. The collaboration and assistance of Reggie T. Kidd, M. Joseph McKenney and Raymond Atherly (Analytical Mech. Assoc.) in design of the benchtop apparatus is greatly appreciated. The assistance of Johnnie West, Sam Pollard and George Hilton (NASA LaRC) in fabrication, assembly and modification of the benchtop assemblies is also gratefully acknowledged. Joe Kain and Carlos Pimental (Johnson Matthey) ably fabricated the shape memory alloy flexures used in this study. Support from NASA's Advanced Air Vehicles Program, Advanced Air Transport Technology Project is also gratefully acknowledged.

References

[1]Choudhari, M. M. and Khorami, M. R., "Effect of Three-Dimensional Shear-Layer Structures on Slat Cove Unsteadiness," *AIAA Journal*, **45**(9)2174-2186, September 2007.

[2]Mau, K. and Dobrzynski, W., "Flexible airflow separator to reduce aerodynamic noise generated by a leading edge slat of an aircraft wing," U.S. Patent No. 6,789,769, 14 September 2004.

[3]Khorrami, M. D., Berkman, M. E., and Choudhari, M., "Unsteady flow computations of a slat with a blunt trailing edge," *AIAA Journal*, Vol. 38, No. 11, 2000, pp. 2050–2058.

[4]Singer, B. A., Lockard, D. P., and Brentner, K. S., "Computational Aeroacoustic Analysis of Slat Trailing-Edge Flow," AIAA Journal, Vol. 38, No. 9, 2000, pp. 1558–1564.

[5]Khorrami, M. R., Singer, B. A., and Berkman, M. E., "Time-accurate Simulations and Acoustic Analysis of Slat Free Shear Layer," *AIAA Journal*, Vol. 40, No. 7, 2002, pp. 1284–1291.

[6]Khorrami, M. R., Singer, B. A., and Lockard, D. P., "Time-accurate Simulations and Acoustic Analysis of Slat Free Shear Layer: Part II," AIAA Paper 2002-2579, 2002.

[7]Khorrami, M.R. and Lockard, D.P., "Effects of Geometric Details on Slat Noise Generation and Propagation," AIAA Paper 2006-2664, 2006.

[8]Gleine, W., Mau, K., and Carl, U., "Aerodynamic Noise Reducing Structure for Aircraft Wing Slats," US Patent No. US 6,394,396 B2, 28 May 2002.

[9]Streett, C. L., Casper, J. H., Lockard, D. P., Khorrami, M. R., Stoker, R. W., Elkoby, R., Wenneman, W. F., and Underbrink, J. R., "Aerodynamic Noise Reduction for High-Lift Devices on a Swept Wing Model," AIAA Paper 2006-212, 2006.

[10]Horne, W.C., James, K.D., Arledge, T.K., Soderman, P.T., Burnside, N., and Jaeger, S.M., "Measurements of 26%-scale 777 Airframe Noise in the NASA Ames 40- by 80 Foot Wind Tunnel," AIAA Paper 2005-2810, May 2005.

[11]Imamura, T., Ura, H., Yokokawa, Y., Enomoto, S., Yamamoto, K., and Hirai, T., "Designing of Slat Cove Filler as a Noise Reduction Device for Leading-edge Slat," AIAA Paper 2007-3473, 2007.

[12]Turner, T. L.; Kidd, R. T.; Hartl, D. J.; and Scholten, W. D.: "Development of a SMA-Based, Slat-Cove Filler for Reduction of Aeroacoustic Noise Associated with Transport-Class Aircraft Wings," *Proc. ASME 2013 Conf. on Smart Matl., Adaptive Struct. and Intell. Sys.*, SMASIS2013-3100, Snowbird, UT, September 16-18, 2013.

[13]Scholten, W. D.; Hartl, D. J.; and Turner, T. L.: "Analysis-Driven Design Optimization of a SMA-Based Slat-Cove Filler for Aeroacoustic Noise Reduction," *Proc. ASME 2013 Conf. on Smart Matl., Adaptive Struct. and Intell. Sys*., SMASIS2013-3104, Snowbird, UT, September 16-18, 2013.

[14]Scholten, W. D.; Hartl, D. J.; and Turner, T. L.: "Development and Analysis-Driven Optimization of a Superelastic Slat-Cove Filler for Airframe Noise Reduction," *AIAA Journal*, 54(3) 1074-1090, March 2016, doi: 10.2514/1.J054011.

[15]Scholten, W. D.; Hartl, D. J.; Turner, T. L.; and Strganac, T. W.: "Reduction of Actuation Loads in a Self-Deploying SMA-Based Slat-Cove Filler for a Transport Aircraft," *Proc. ASME 2015 Conf. on Smart Matl., Adaptive Struct. and Intell. Sys*., SMASIS2015-9015, Colorado Springs, CO, 21-23 September 2015.

[16]Scholten, W.; Patterson, R.; Hartl, D.; Strganac, T.; Volpi, J.; Chapelon, Q.; and Turner, T.: "Noise Reduction in a High-Lift Wing using SMAs: Computational Fluid-Structural Analysis," *Proc. ASME 2016 Conf. on Smart Matl., Adaptive Struct. and Intell. Sys.*, SMASIS2016-9196, Stowe, VT, 28-30 September 2016.

[17]Qureshi, H., Hamdani, H. R., and Parvez, K., "Effects on Dynamic Stall on Cambered Airfoil with Drooping Leading Edge Control," AIAA Paper 2006-1064, 2006.

[18]Hileman, J. I., Reynolds, T. G., de la Rosa Blanco, E., Law, T. R., and Thomas, S., "Development of Approach Procedures for Silent Aircraft," AIAA Paper 2007-451, 2007.

[19]Khodadoust, A. and Washburn, A., "Active Control of Flow Separation on a High-Lift System with Slotted Flap at High Reynolds Number," AIAA Paper 2007-4424, 2007.

[20]Maldar, A., Arokkiaswamy, A., Gemson, R. M. O., and Sanal Kumar, V. R., "Aerodynamic Sound Reduction for Silent Aircraft," AIAA Paper 2008-150, 2008.

[21]Bain, J. J., Sankar, L. N., Prasad, J. V. R., Bauchau, O. A., Peters, D. A., and He, C., "Computational Modeling of Variable-Droop Leading Edge in Forward Flight," *Journal of Aircraft,* Vol. 46, No. 2, 2009, pp. 617-626.

[22]Hall, C. A., Schwartz, E., and Hileman, J. I., "Assessment of Technologies for the Silent Aircraft Initiative," *Journal of Propulsion and Power*, Vol. 25, No. 6, December 2009, pp. 1153-1162.

[23]Bahr, C. J.; Hutcheson, F. V.; Thomas, R. T.; and Housman, J. A.: "A Comparison of the Noise Characteristics of a Conventional Slat and Krueger Flap," AIAA-2016-2961.

[24]Turner, T. L. and Long, D. L.; "Development of a SMA-Based, Slat-Gap Filler for Airframe Noise Reduction," AIAA-2015-0730, AIAA SciTech 2015 Forum, Kissimmee, Florida, 5-9 January 2015.

[25]Auricchio, F. and Taylor, R. L.: "Shape-memory alloys: modelling and numerical simulation of the finite-strain superelastic behavior," *Computer Methods in Applied Mechanics and Engineering*, 143(1-2) 175-194, 15 April 1997.

[26]Auricchio, F., Taylor, R. L. and Lubliner, J.: "Shape-memory alloys: macromodelling and numerical simulation of the superelastic behavior," *Computer Methods in Applied Mechanics and Engineering*, 146(3-4)281-312, 15 July, 1997.